BJP British Journal of Pharmacology

DOI:10.1111/bph.13162
www.brjpharmacol.org

RESEARCH PAPER

Dynasore enhances the formation of mitochondrial antiviral signalling aggregates and endocytosis-independent NF-κB activation

M Ailenberg[1,2,3], C Di Ciano-Oliveira[1,2,3], K Szaszi[1,2,3], Q Dan[1,2,3], M Rozycki[1,2,3], A Kapus[1,2,3] and O D Rotstein[1,2,3]

[1]*Departments of Surgery, St. Michael's Hospital, Toronto, ON, Canada,* [2]*University of Toronto, Toronto, ON, Canada, and* [3]*Keenan Research Centre for Biomedical Science, St. Michael's Hospital, Toronto, ON, Canada*

Correspondence
Ori D. Rotstein, St. Michael's Hospital, 30 Bond Street, 16CC-044, Toronto, Ontario, Canada M5B 1W8. E-mail: rotsteino@smh.ca

Received
29 September 2014
Revised
18 February 2015
Accepted
31 March 2015

BACKGROUND AND PURPOSE

Dynasore has been used extensively as an inhibitor of clathrin-mediated endocytosis. While studying the role of endocytosis in LPS-induced signalling events, we discovered that dynasore itself induced activation of NF-κB, independently of its effects on endocytosis and without involving the Toll-like receptor 4 signalling pathways. The purpose of this study was to characterize this novel effect and to explore the underlying mechanism of action.

EXPERIMENTAL APPROACH

We utilized gel electrophoresis, microscopy, gene knockdown and luciferase-based promoter activity to evaluate the effect of dynasore on cell signalling pathways and to delineate the mechanisms involved in its effects,

KEY RESULTS

Dynasore activated the NF-κB and IFN-β pathways by activating mitochondrial antiviral signalling protein (MAVS). We showed that MAVS is activated by NOX/Rac and forms high molecular weight aggregates, similar to that observed in response to viral infection. We also demonstrated that dynasore-induced activation of JNK occurs downstream of MAVS and is required for activation of NF-κB and IFN-β.

CONCLUSION AND IMPLICATIONS

These findings demonstrate a novel effect of dynasore on cell signalling. We describe a novel Rac1-, ROS- and MAVS-mediated signalling cascade through which dynasore dramatically activates NF-κB, mimicking the viral induction of this key inflammatory signalling pathway. Our results call attention to the need for a broader interpretation of results when dynasore is used in its traditional fashion as an inhibitor of clathrin-mediated endocytosis. These results suggest the intriguing possibility that dynasore or one of its analogues might be of value as an antiviral therapeutic strategy or vaccine adjuvant.

Abbreviations

CME, clathrin-mediated endocytosis; DRP1, dynamin-related protein 1; MAVS, mitochondrial anti-viral signalling; MFN, mitofusin; ROS, reactive oxygen species; SAPK, stress-activated PK (JNK2); TLR4, Toll-like receptor 4

Tables of Links

TARGETS	
Catalytic receptors[a]	**Enzymes**[b]
TLR4	DRP1 (DAPK2)
	JNK1
	JNK2 (SAPK)

LIGANDS		
ATF-2 (GDNF)	Rac1	SP600125
H_2O_2	Rac2	TGFβ
IFN-β	Rac3	Wnt-5a
LPS	Rhodamine	

These tables list key protein targets and ligands in this article which are hyperlinked to corresponding entries in http://www.guidetopharmacology.org, the common portal for data from the IUPHAR/BPS Guide to PHARMACOLOGY (Pawson *et al.*, 2014) and are permanently archived in the Concise Guideto PHARMACOLOGY 2013/14 ([a,b]Alexander *et al.*, 2013a,b).

Introduction

Dynasore is a cell-permeant inhibitor of the GTPase activity of dynamin 1, dynamin 2 and the mitochondrial dynamin isoform dynamin-related protein 1 (DRP1; Macia *et al.*, 2006). It has been extensively used to investigate the role of clathrin-mediated endocytosis (CME) in a plethora of cellular processes (Kirchhausen *et al.*, 2008), including surface receptor trafficking and its impact on the ensuing downstream signalling. For example, dynasore has been reported to facilitate pathways involved in TGFβ-induced Plasminogen activator inhibitor-1 (PAI-1) expression (Chung *et al.*, 2009). These results were interpreted in terms of the inhibitory effect of dynasore on endocytosis, although the mechanism has not been investigated.

In previous work we explored the effect of oxidative stress on Toll-like receptor 4 (TLR4) signalling and trafficking of the receptor (Szászi *et al.*, 2005; Powers *et al.*, 2006; Papia *et al.*, 2011). In the course of our studies investigating the role of endocytosis in TLR4-dependent NF-κB signalling, we found that dynasore itself was able to activate both NF-κB and Interferon regulatory factor-3 (IRF-3) pathways in the absence of LPS and independently of its effects on dynamin and endocytosis. This suggested that dynasore exerts significant, hitherto unrecognized effects on various signalling pathways. In addition to TLR4 signalling, the mitochondrial antiviral signalling (MAVS) protein has also been implicated as an upstream regulator of NF-κB, we determined whether dynasore might affect this key inflammatory pathway by modulating MAVS signalling. MAVS is recognized as a central molecule in the host's antiviral response through its ability to regulate the activation of NF-κB and IRF-3 and downstream gene expression (Seth *et al.*, 2005). It has been explored as a potential therapeutic target in viral infection (Xu *et al.*, 2014). In our subsequent investigations, we showed that dynasore exerted these effects on NF-κB and IRF-3 pathways through activation of the mitochondrial adaptor protein MAVS and this involved upstream activation of the small G-protein Rac1 and the induction of reactive oxygen species (ROS). Together, these findings not only elucidate a new mechanism whereby dynasore affects cell signalling, but also suggest the need for a broader interpretation of results when dynasore is used in its traditional fashion as an inhibitor of CME.

Methods

Cell culture

RAW 264.7 and HEK cells were purchased from ATCC (Manassas, VA, USA) and maintained in D-MEM containing 10% FBS as previously described (Powers *et al.*, 2006). Cells were passaged every week for a maximum of 15 passages. For all experiments, 24 h after plating, cells were starved in 2% FBS for 24 h before starting the experiment.

Endotoxin removal with polymyxin B

Ten microlitre aliquots of polymyxin B were added to samples containing treatments [dynasore, DMSO or LPS (LPS from *Escherichia coli* 0111:B4)] and incubated at room temperature for 30 min. Treatments were added to cells previously transfected with NF-κB-luc and Renilla-luc for 24 h. Cells were then processed for luciferase reporter activity as described in the succeeding text.

Transfection of plasmids and siRNA

Plasmids or siRNA were transfected using jetPRIME™ reagent (Polyplus transfection, New York, NY, USA) according to the manufacturer's recommendations. Plasmids pGL8XNF-κB-fos-luc (from Drs Tak Mak and Dirk Brenner from the Princess Margaret Hospital Toronto, ON, Canada), pGL3-INFβ- luc (from Drs John Hiscott of McGill University and Marc Servant of Université de Montréal, QC, Canada), pcDNA3 vector containing a dominant-negative mutant of dynamin (DynK44A), tagged with an HA epitope at its amino terminus (from Dr. S. Schmid; Scripps Institute, La Jolla, CA, USA) and Mito-RFP (Red fluorescent protein; Clontech, Mountain View, CA, USA) were used at 400 ng·mL^{-1}. The thymidine kinase minimal promoter-driven renilla luciferase internal control plasmid pRL-TK was purchased from Promega (Madison, WI, USA) and transfected at 40 ng·mL^{-1}. Qiagen (Toronto, ON, Canada) negative control (1027280) and MAVS (S100970151) siRNAs were used at 10 nM (final concentration). We initially evaluated four different MAVS siRNA and chose one that localized to the 3′-non-translated region of MAVS (5′-CCACAC ATACATGCTAATATA-3′). We initially evaluated two different siRNAs for Rac 1 and Rac 2 and chose one siRNA for each isoform. Rac and negative control siRNA were transfected at a final concentration of 40 nM [Rac1 siRNA

(S100181370): 5′-GGGCGTTGAGTCCATATTTAA-3′, Rac2 siRNA (S100181405): 5′-CAGAACAAATCTACTTCAGTA-3′]. SCBT RIG-I siRNA (61481), a pool of three target-specific siRNAs, was transfected at a final concentration of 40 nM (5′-CCAUGCAACAUAUCUGUAA-3′, 5′-CGAGGAACUUGGA AAGCUU-3′, 5′-CAAGAAGAGUACCACUUAA-3′). K44A plasmid and siRNA were transfected 24 h before luciferase transfection. For Western studies, siRNA was transfected 24 h before treatments.

Luciferase reporter assay

Luciferase reporter assays were performed as previously described (Masszi *et al.*, 2010) with modification. Briefly, cells were plated in 24-well tissue culture plates at a density of 2×10^5 cells per well overnight and then starved with 2% FBS in DMEM. Next day, cells were transfected with reporter plasmids for 6 h. Cells were pretreated with the inhibitors in HBSS for 15–30 min followed by treatments in 2% FBS in DMEM for 24 h. Cells were then lysed with 100 µL lysis buffer (Promega) and 20 µL were assayed directly for firefly and renilla luciferase levels utilizing dual-luciferase reporter assay system (Promega) with tube luminometer (Berthold Technologies, Bad Wildbad, Germany). Data were normalized by division of firefly luminescence with that of renilla and expressed as fold of untreated control.

Detection of H_2O_2 in RAW cells conditioned media

Hydrogen peroxide levels in conditioned media of RAW cells were measured using Amplex red hydrogen peroxide/peroxidase assay kit (Molecular Probes). Cells were plated and treated as described earlier in 24-well plates. Fifty microlitre aliquots of conditioned medium were assayed in duplicates. A standard curve for H_2O_2 was assayed in parallel. H_2O_2 levels are expressed as µmol per 2×10^5 cells.

SDS-PAGE and Western blotting

Cells were lysed with lysis buffer and subjected to Western blotting as previously described (Powers *et al.*, 2006). Protein concentrations were measured using DC protein assay (Bio-Rad, Mississauga, ON, Canada) and equal protein amounts were loaded on gel. Gel loading was assessed by probing for GAPDH, actin or corresponding non-phosphorylated proteins. Protein signals were developed using Enhanced chemiluminescence (ECL) or ECL Prime (GE Healthcare Life Sciences, Baie d'Urfe, QC, Canada) and captured on film. Protein signal intensities were compared using GS calibrated densitometer (Bio-Rad). Where indicated, bands taken from non-contiguous lanes of the *same* blot are indicated by insertion of dividing lines.

Cell fractionation

Cytoplasmic and nuclear cell fractions were isolated using NE-PER stepwise separation (Pierce, Rockford, IL, USA) as previously described (Masszi *et al.*, 2010).

Rac activity assay

Active (GTP-bound) Rac was captured using Glutathione S-transferase- Rac/Cdc42 (p21) binding domain (GST- PBD) as described previously (Waheed *et al.*, 2013). Briefly, RAW cells grown on 10 cm dishes were starved in 2% FBS overnight and then treated with dynasore (80 µM) for the times indicated in the figure. Cells were lysed with ice-cold Rac assay buffer containing 25 mM HEPES (pH 7.5), 150 mM NaCl, 1% NP-40, 10% glycerol, 10 mM $MgCl_2$, 1 mM EDTA, 1 mM Na_3VO_4, 1 mM PMSF, 25 mM NaF and protease inhibitors. After centrifugation, aliquots for determination of total Rac were removed. The remaining supernatants were incubated at 4°C for 45 min with 20–25 µg of GST-PBD beads followed by extensive washing. Total cell lysates and the PBD- captured proteins were analysed by Western blotting using Rac1/2/3 antibody. Results were quantified by densitometry.

Semi-denaturing detergent-agarose gel electrophoresis (SDD-AGE)

To measure high molecular weight aggregates, SDD-AGE (Bagriantsev *et al.*, 2006) was employed with modifications. Briefly, cell extracts were incubated at room temperature for 5 min with 0.5% SDS (final concentration) followed by addition of 6× DNA loading dye (Fermentas, Burlington, ON, Canada). Samples were loaded on 1.5% agarose gel containing 0.1% SDS and resolved using 1X Tris/Borate/EDTA (TBE) running buffer containing 0.1% SDS at 100 V in the cold. Protein aggregates were transferred to nitrocellulose paper with PBS using capillary transfer. After transfer, nitrocellulose membrane was subjected to immunoblotting as described earlier in the SDS-PAGE section.

Immunofluorescence, rhodamine-transferrin uptake by cells and mitochondria labelling by Mito-RFP plasmid

Cells were plated on glass coverslips in 10% FBS. Next day, cells were starved with 2% FBS for additional 24 h. For the rhodamine-transferrin (Life Technologies Inc.) uptake study, cells were treated for 15 min in HBSS with the inhibitors. Cells were then allowed to bind rhodamine-transferrin on ice and transferred to 37°C for 5 min. NF-κB p65 and MAVS immunocytochemistry was performed as described earlier (Masszi *et al.*, 2010). Images were taken using Olympus IX81 fluorescent microscope (Olympus America Inc., Melville, NY, USA). To quantify NF-κB p65 translocation to the nucleus, 100 cells in each field were assessed and counted for NF-κB p65 localization to the cytoplasm, nucleus or both. Mito-RFP plasmid was transfected as described earlier. Cells where then treated and processed as described in the relevant figure legend. Images were taken using Zeiss LSM 700 inverted confocal microscope. Three-dimensional (3D) surface rendering of confocal microscopy imaging was performed with Imaris 7.7.0 software (Bitplane AG, Zurich, Switzerland). Nuclear staining was performed using Hoechst 33342 (Life Technologies Inc.).

Trypan Blue dye exclusion assay

RAW cells (5×10^4 per 200 µL) were plated in 48-well plates. Next day, cells were treated in 2% FBS with the inhibitors for 2 or 24 h. Cells were stained with a 0.04% (final concentration) Trypan Blue in PBS buffer. Cells were washed with PBS and stained; cells were counted in a field of 1000 cells. Viable cells that excluded the dye are expressed as percentage of live cells.

Statistical analysis

Data were subjected to ANOVA. Differences between means were evaluated using Tukey–Kramer minimum significant differences and significance was set to $P < 0.05$. When applicable, means were compared using Student's *t*-test. Bars represent mean plus SEM. Asterisks denote statistical difference compared with control. When not specified, data represent at least three experiments.

Reagents and antibodies

All reagents were purchased from Sigma-Aldrich (Oakville, ON, Canada) unless otherwise stated. Primary antibodies were purchased from Cell Signaling (Pickering, ON, Canada), Santa Cruz Biotechnology (SCBT; Paso Robles, CA, USA) or Sigma-Aldrich. Cell Signaling primary antibodies and catalogue numbers: DRP1 (8570), p-DRP1 (Ser^{637}; 4867), GAPDH (5174), IκBα (4812), MAVS (4983), NF-κB p65 (3987), NF-κB p-p65 (Ser^{536}; 3033), RAC1/2/3 (2465). SCBT primary antibodies and catalogue numbers: histone (10806), stress-activated PKs (SAPK)/JNK2 (7345), p-SAPK/JNK (6254), RIG-I (376845). Sigma antibody and catalogue number: β-actin (A5316). HRP-conjugated anti-rabbit or anti-mouse secondary antibodies where from Jackson Immuno Research Laboratories (Baltimore, PA, USA; 711035152 and 715035151 respectively). Anti-rabbit Alexa Fluor 568 and 488 IgGs were products of Molecular Probes (Life Technologies Inc., Burlington, ON, Canada; A-10042 and A-21206 respectively).

Results

Dynasore induces NF-κB activation

During our studies investigating the role of endocytosis in LPS-mediated TLR4 signalling (Ailenberg and Rotstein, 2011), we used dynasore to inhibit dynamin 2 and thus CME (Ailenberg *et al.*, 2011). Based on a prior report (Husebye *et al.*, 2006), we had expected enhanced activation of the MyD88-Mal pathway following LPS treatment of RAW cell in the presence of dynasore, presumably because CME inhibition by dynasore blocks the TRAM-TRIF pathway thus diverting and augmenting the LPS signal through the MyD88-MAL pathway. Indeed, treatment of RAW cells with combination of LPS and dynasore enhanced NF-κB activation as measured by NF-κB-luciferase (Figure 1A). Surprisingly, dynasore alone also enhanced NF-κB -dependent luciferase activation (Figure 1A). We asked whether LPS contamination of the dynasore reagent might have contributed to the activation of NF-κB. The addition of the LPS-neutralizing reagent polymyxin B to dynasore did not prevent its ability to induce NF-κB activation, while it abolished the ability of LPS to do so (Figure 1B). In order to rule out protein agonist contamination in the dynasore preparation, dynasore solutions were boiled for 10 min and then added to cells and processed as earlier. No reduction in NF-κB-luciferase activation was noted in boiled dynasore compared with non-boiled dynasore (not shown). In addition, dynasore did not cause false-positive luminometry readings, as dynasore or DMSO added to extracts of cells previously transfected with NF-κB and renilla-luciferase plasmids for 24 h showed no increase in luminescence (not shown). Hydroxy-dynasore (OH-dynasore), a dynasore analogue, with increased potency for CME inhibition (Howes *et al.*, 2012), also induced NF-κB-luciferase (Figure 1C), albeit was not as potent as the parent compound. Similarly, in untransfected RAW 264.7 cells, dynasore alone also activated NF-κB, as demonstrated by its ability to induce p65 phosphorylation and IκBα degradation (Figure 1D–F) as well as translocation to the nucleus both by Western blot analysis and immunofluorescence (Figure 2A and B respectively). While we did not examine the kinetics of p65 translocation to the nucleus, the immunofluorescence studies suggest that both LPS and dynasore cause robust movement of p65 to the nuclear compartment (Figure 2C). At the time point examined, translocation of p65 to the nucleus was more complete in LPS-treated cells, accounting for their ability to more completely obscure the nuclear Hoechst staining (Figure 2B – middle vs. right panel). This is quantitated in Figure 2C.

Having shown the ability of dynasore to induce NF-κB activation, we explored potential mechanisms underlying its effect. First, the dynasore-induced activation of NF-κB was not mediated by the drug's ability to inhibit CME *per se*. While other CME inhibitors (MiTMAB, Pitstop-2) inhibited rhodamine-transferrin endocytosis in RAW cells to a similar extent as dynasore (Supporting Information Fig. S1A), these agents, unlike dynasore, did not cause p65 NF-κB activation (Supporting Information Fig. S1B,C) or IκBα degradation (Supporting Information Fig. S1C). It should be noted that all the inhibitors tested did not affect cell viability after 2 h of treatment (maximum treatment duration of Western blot experiments; Supporting Information Fig. S1D). However, after 24 h treatment (duration of luciferase-based experiments; Supporting Information Fig. S1E), viability of control, dynasore, Pitstop-2 and MiTMAB-treated cells were 99.6%, 99.3%, 62.0% and 0% respectively. Therefore, the effect of MiTMAB was studied by Western blot at t = 2h and not in luciferase assay. The effects of dynasore and Pitstop-2 were assessed in both time frames. Although Pitstop-2 *did* affect to some extent cell viability at 24 h (62%), the changes in cell viability were offset by normalizing NF-κB-luciferase values to renilla-luciferase values. Further, inhibition of dynamin using the dominant-negative dynamin-2 K44A failed to activate NF-κB- luciferase (not shown). Dynasore could potentially activate the TLR-4 pathway through general inhibition of endocytosis by causing TLR4 receptor oligomerization and augmented signalling via the MyD88-Mal pathway (Bonham *et al.*, 2014). However, blocking the LPS-MyD88-Mal pathway with IRAK-1/4 inhibitor had no effect on dynasore-induced NF-κB activation, while it significantly reduced LPS-induced signalling (Supporting Information Fig. S2A). To further investigate the role of TLR4 in dynasore-induced activation of NF-κB, we studied dynasore's effect in HEK cells that do not express TLR4. Supporting Information Fig. S2B shows that dynasore induces robust activation of NF-κB in these cells. Considered in aggregate, these studies demonstrate that dynasore is able to induce activation of the NF-κB signalling pathway, independent of its effect on endocytosis and via a pathway that does not involve TLR4 activation.

Role of MAVS in downstream effects of dynasore

Having shown that activation of NF-κB by dynasore occurs independent of the TLR4-MyD88 pathway, we investigated

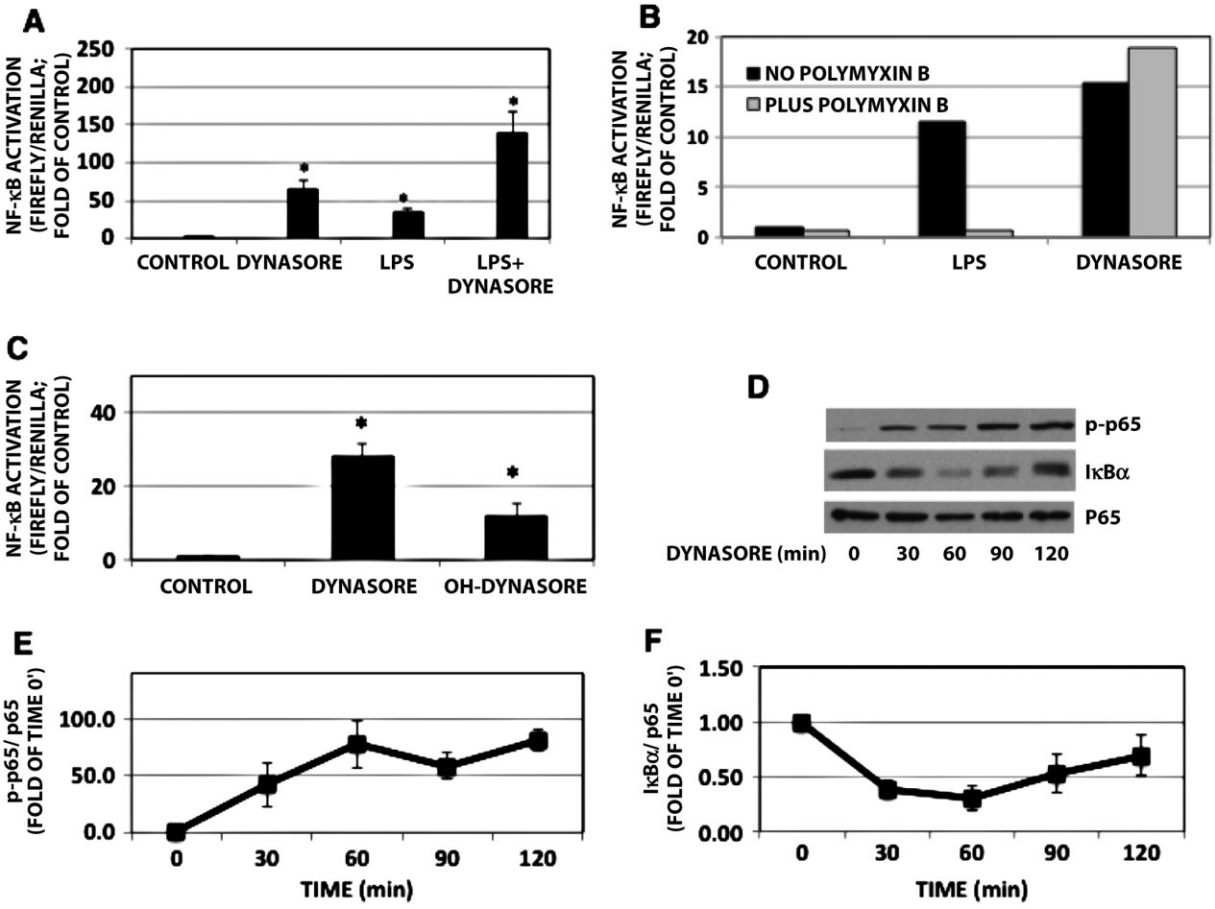

Figure 1

Dynasore influences NF-κB pathway in cultured RAW 264.7 cells. (A) NF-κB-luciferase: cells were pretreated with 80 μM dynasore or DMSO in HBSS for 15 min and then treated overnight with dynasore or LPS (15 ng·mL^{-1}) in 2% FBS. All treatments induced statistically different effects from untreated control, denoted by asterisk. Dynasore or LPS treatments are also induced statistically different results from dynasore+ LPS treatment. ANOVA: $P < 3 \times 10^{-7}$; d.f. within groups = 76. (B) NF-κB-luciferase: polymyxin B did not affect dynasore's ability to induce NF-κB-luciferase activation, but reduced LPS-induced activation of NF-κB-luciferase. (C) NF-κB-luciferase assay: cells were treated with DMSO, dynasore or OH-dynasore. (ANOVA: $P < 4 \times 10^{-4}$; d.f. within groups = 7). (D) Western blot: RAW cells were treated with dynasore for the times indicated. (E) Summary of densitometry results of experiments depicted in panel D. Values of NF-κB p-p65 normalized to p65 to compensate for loading errors. ANOVA: $P <$ 0.008; d.f. within groups = 10. (F) Summary of densitometry results of experiments depicted in panel D. Values of IκBα were normalized to p65 to compensate for loading errors. ANOVA: $P < 0.008$; d.f. within groups = 20. Note the induction in p65 phosphorylation by dynasore, presumably by inducing degradation of IκBα.

other potential signalling pathways. The protein MAVS is known to participate in the antiviral response through its involvement as a signalling platform for downstream events, leading to activation of NF-κB and phosphorylation of IRF-3. Together, these transcription factors induce activation of type 1 IFN genes and subsequent antiviral activity. In addition to activating NF-κB and consistent with signalling via MAVS activation, dynasore also induced IFN-β-luciferase promoter activity (Figure 3).

The biochemical hallmark of MAVS activation by viruses is the apparent reduction in the level of MAVS on SDS-PAGE due to resistance of active MAVS to detergent extraction (Seth *et al.*, 2005). Remarkably, dynasore caused ~90% reduction in the level of monomeric MAVS over 120 min exposure (Figure 4A and B). Dynasore also caused a reduction in MAVS levels and induced degradation of IκBα in a dose-dependent fashion (Figure 4C and D).

One potential reason for the reduction in MAVS monomer content could be the proteasomal degradation of this protein. In favour of this possibility, it has been shown that viral proteins can induce proteosomal degradation of MAVS as a mechanism whereby they thwart efficient host response (Castanier *et al.*, 2012). As shown in Figure 4E, MG-132 had no effect on the reduction in MAVS protein, whereas it clearly prevented degradation of IκBα, a protein known to undergo proteosomal degradation in response to phosphorylation.

The other possibility is that the decrease in monomer concentration is due to the oligomerization and aggregation of MAVS. The work by Chen *et al.* demonstrated that MAVS activation leads to the formation of prion-like aggregates, which provoke downstream antiviral activity (Hou *et al.*, 2011). In their system, this occurred concomitant with a reduction in monomeric MAVS protein (Seth *et al.*, 2005). We

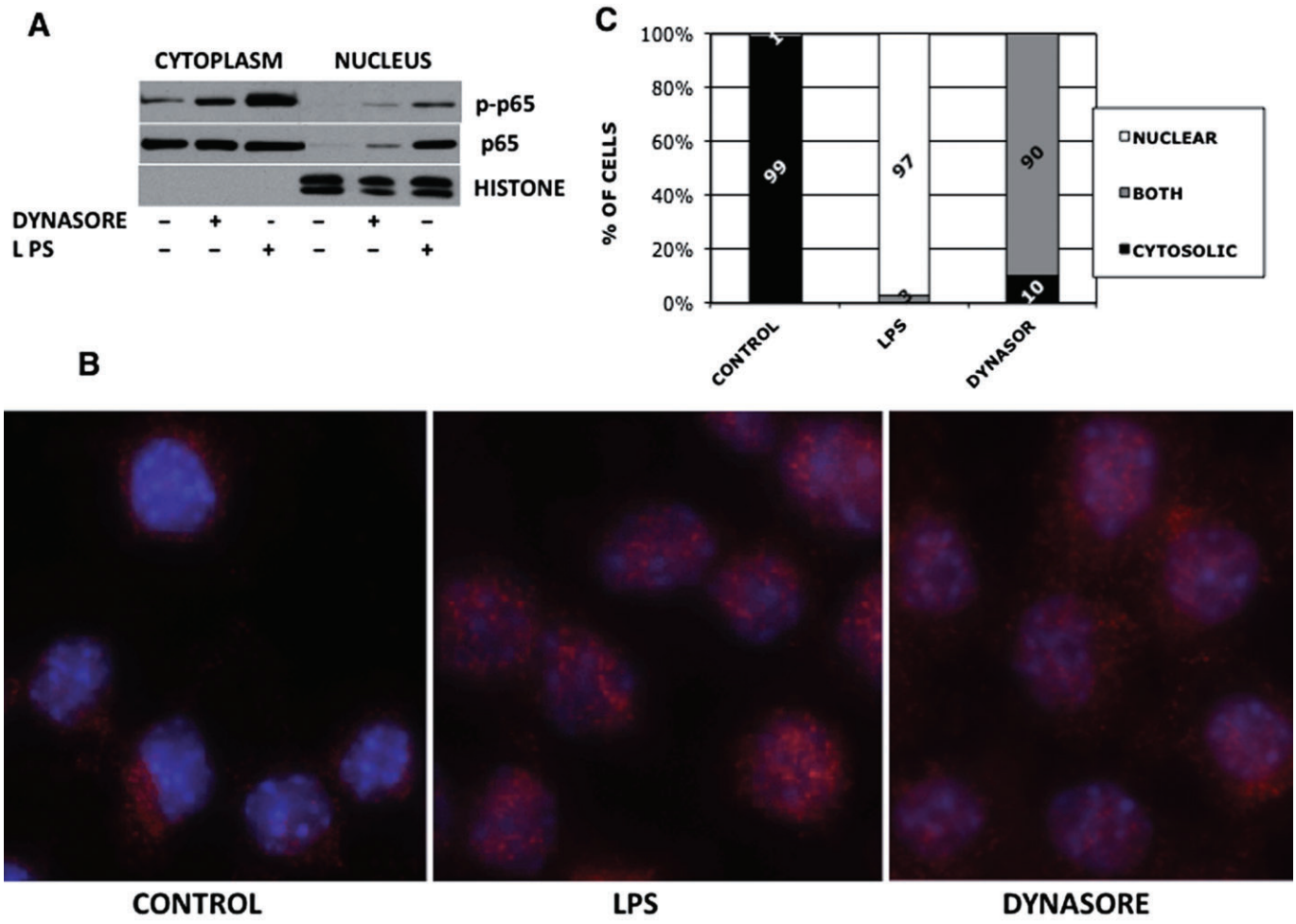

Figure 2

NF-κB p65 translocates to the nucleus following treatment with dynasore. (A) Western blot: RAW cells were treated with 80 μM dynasore or DMSO in HBSS for 90 min. As a positive control for p65 translocation, cells were treated with 15 ng·mL^{-1} LPS. Cytoplasm and nuclear extracts' purity were assessed by reprobing using an antibody against nuclear histones. (B) Immunocytochemistry: RAW cells were plated on coverslips, dynasore was added for 2 h and LPS-positive control was treated for 15 min. Cells were immunostained with anti-NF-κB p65 antibody followed by anti-rabbit Alexa-568 conjugated antibody (red). Hoechst 33342 was used for nuclear staining (blue). (C) To quantify the data in section B, 100 cells in each field were counted for NF-κB p65 localization to the cytoplasm, nucleus or both. Note that while in 99% of control cells NF-κB p65 was localized to the cytoplasm, 90% and 99% of dynasore and LPS-treated cells, respectively, had NF-κB p65 localized to the nucleus. However, while LPS-treated cells localized NF-κB p65 exclusively to the nucleus, the majority of dynasore-treated cells exhibited NF-κB p65 localization to both the cytoplasm and nucleus.

therefore hypothesized that dynasore might induce formation of these aggregates. Figure 5A demonstrates that dynasore induces the formation of high molecular weight aggregates on SDD-AGE gels, consistent with their characteristic detergent-resistant nature. In agreement with the prior observation that the detergent-resistant aggregates contain disulfide bonds, treatment of the extract with β-mercaptoethanol caused disappearance of the aggregate and restoration of the monomeric MAVS (not shown). The clustering of MAVS protein observed by immunofluorescence microscopy following dynasore treatment also reflects the formation of these aggregates: the elongated thread-like configuration of the mitochondria observed in the control DMSO-treated cells was shortened and formed shorter somewhat circular structures following exposure to dynasore for 15 and 30 min (Figure 5B, IF-MAVS). These MAVS puncta are similar to those observed in virus-infected cells (Xu *et al.*, 2014). Moreover, dynasore treatment altered both the mitochondrial morphology and the relationship between MAVS and mitochondria (Figure 5B, 3D surface rendering and Supporting Information Fig. S3). In the control cells, MAVS was evenly distributed on the surface of the mitochondria (Figure 5B, 3D surface rendering and Supporting Information Fig. S4) and mitochondria were arranged in thread-like structure (Figure 5B, 3D surface rendering and Supporting Information Figs S3 and S4). After treatment with dynasore, MAVS underwent polarized redistribution and localized between adjacent mitochondria or alongside the mitochondria (Figure 5B, 3D surface rendering and Supporting Information Figs S3 and S4), while mitochondria assumed a multi-

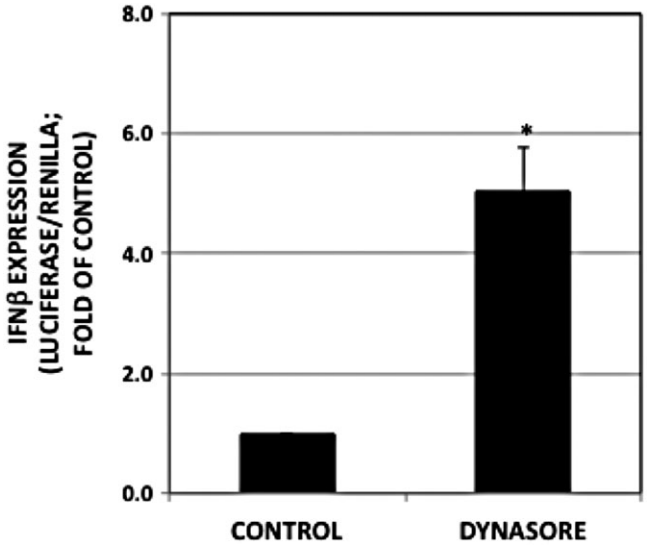

Figure 3

Dynasore induces IFN-β-luciferase promoter activity. RAW cells were maintained and treated as described in the Methods section ($P < 2 \times 10^{-5}$; $n = 12$).

organelle configuration, which seemed to be held together by dynasore-induced MAVS aggregates (Figure 5B, 3D surface rendering, arrows). Together, these findings suggest that dynasore is able to induce a shift in MAVS to the large molecular weight aggregate concomitant with altered mitochondrial distribution, as is observed following viral treatment. These aggregates are considered to act as platforms for the formation of signalosomes and subsequent downstream signalling events. Therefore, to discern the role of MAVS in NF-κB activation in response to dynasore, we transfected cells with MAVS siRNA and treated them with dynasore. MAVS siRNA caused ~50% reduction in MAVS protein (Figure 6A). This intervention caused a significant (and proportional) reduction (55%) in dynasore-induced activation of NF-κB luciferase activity (Figure 6B).

As noted earlier, dynasore was initially discovered through a screen for inhibition of GTPase activity of dynamin 1 and has been employed as an agent to study CME. It was also shown to inhibit the GTPase activity of the mitochondrial dynamin DRP1, although the physiological consequences of dynasore on DRP1 have not been investigated (Macia *et al.*, 2006). Our initial studies showed that treatment of RAW cells with dynasore caused a rapid time-dependent phosphorylation of DRP1 on Ser637 (Supporting Information Fig. S5A and B) that was accompanied with activation of MAVS, as evidenced by reduction in MAVS levels (see Figure 4A and B). However, the effect of dynasore did not seem to be due to inhibition of DRP1 GTPase activity, as treatment with a specific DRP1 GTPase inhibitor MIDVI-1 did not elicit similar effects as dynasore. Specifically, MIDVI-1 alone did not recapitulate dynasore's effect on DRP-1 phosphorylation (Supporting Information Fig. S5C and D) nor did it alter the effect of dynasore on MAVS monomer reduction (Supporting Information Fig. S5C and E).

The effect of dynasore is mediated through ROS

ROS can contribute to the activation of a number of signal transduction pathways and they have been shown to impact MAVS activation (West *et al.*, 2011; Finkel, 2012). Pretreatment of RAW cells with the antioxidant N-acetylcysteine (NAC), lessened dynasore-induced phosphorylation of NF-κB protein p65 and dynasore-induced activation of NF-κB-luciferase in a dose-related fashion (Figure 7A and B). Dynasore-induced degradation of IκBα was lessened when cells were pretreated with NAC (Figure 7A, lower two panels). NAC had no effect on cell viability after 2 h (Supporting Information Fig. S1D) or 24 h (Supporting Information Fig. S1E).

Consistent with a role for ROS, dynasore was able to induce H_2O_2 release into conditioned medium of RAW cells (Figure 7C). Treatment of RAW cells with H_2O_2 reduced MAVS monomer and also enhanced p-DRP1 (see also Supporting Information Fig. S5) similar to the effect of dynasore (Figure 7D–F). To discern the potential source of ROS, we used specific inhibitors of ROS production. Both Mito-Tempo and apocynin were able to inhibit dynasore-induced activation of NF-κB-luciferase, suggesting that both mitochondrial oxidases and NADPH oxidase contribute to the signalling effects of dynasore (Figure 7G).

The role of Rac activation in dynasore-induced activation of MAVS and NF-κB

Rac activation results in generation of ROS, both through its association and activation of NADPH oxidase (Hordijk, 2006) and, as demonstrated recently, via activation of the mitochondrial electron transport chain (Osborn-Heaford *et al.*, 2012). Given the ability of inhibitor of both mitochondrial and cytosolic antioxidants to mitigate the effect of dynasore on NF-κB activation (Figure 7G), we examined the effect of dynasore on Rac activation and its potential downstream events. As shown in Figure 8A and B, dynasore induced a rapid activation of Rac followed by a diminution over 30 min.

Using isotype-specific siRNAs (Figure 8C), Rac1 siRNA, but not Rac2 siRNA, prevented the dynasore-induced reduction in monomeric MAVS (Figure 8D and E) and the activation of NF-κB-dependent reporter construct (Figure 8F).

Activated Rac is also known to lead to activation of SAPK/JNK (Sanada *et al.*, 2008). Figure 9A shows that dynasore treatment causes a progressive increase in SAPK/JNK phosphorylation. Treatment with NAC prevented dynasore-stimulated phosphorylation of SAPK/JNK (Figure 9A).

Similar to the data shown in Figure 7A, dynasore caused gradual enhancement in phosphorylation of p65 (Figure 9B). Inhibition of activated SAPK/JNK with the inhibitor SP600125 lessened dynasore-induced phosphorylation of p65 and degradation of IκBα (Figure 9B and C) and activation of the NF-κB luciferase (Figure 9D). To discern whether SAPK/JNK activation was up or downstream of MAVS activation, the effect of JNK inhibitor SP600125 on dynasore-induced MAVS activation was studied. The reduction in MAVS caused by dynasore treatment was not inhibited by the presence of SP600125 (Figure 9E). This finding suggests that SAPK/JNK

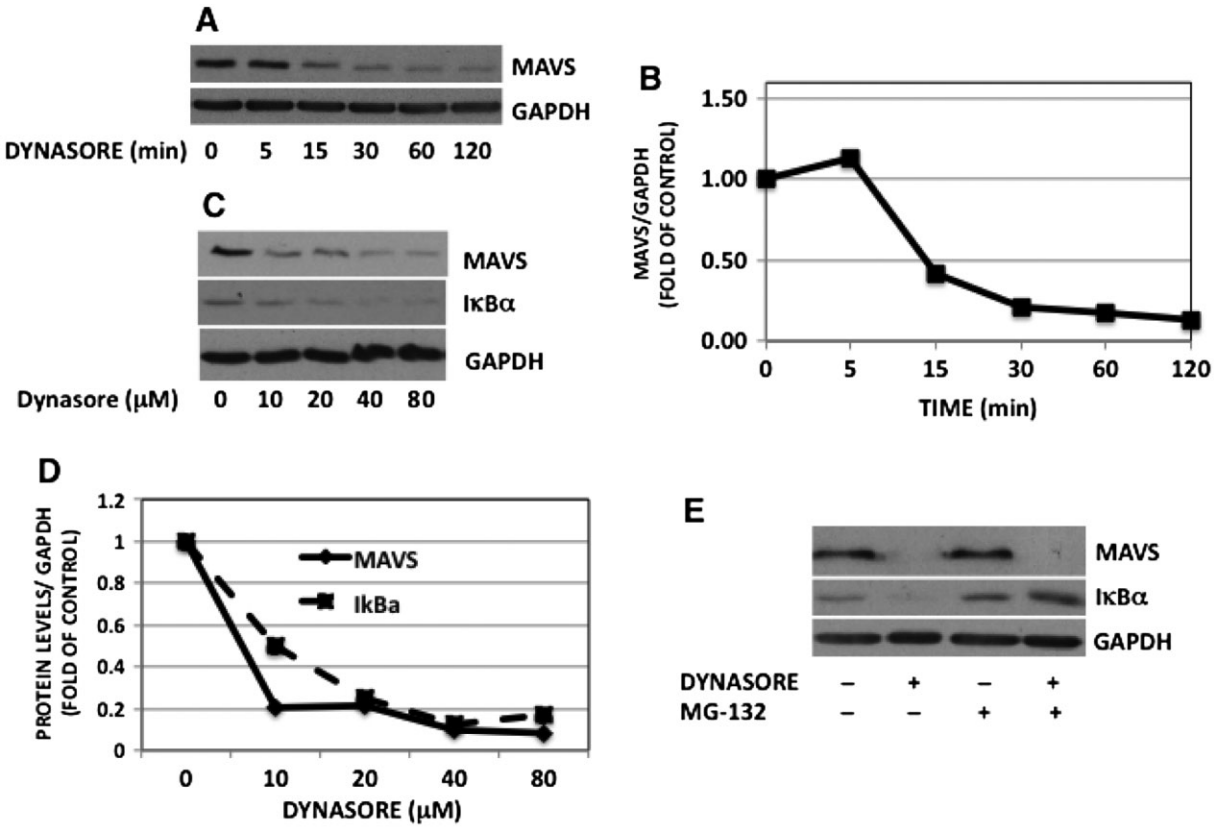

Figure 4

Dynasore induces a reduction in monomeric MAVS independently of proteasome degradation. (A) Cells were pretreated with dynasore (80 μM) or DMSO for the times indicated. Cells were extracted and processed for Western blots. For loading correction, nitrocellulose membranes were reprobed with GAPDH. (B) Bands in panel A were subjected to densitometry and expressed as ratio of MAVS/GAPDH. (C) Cells were treated with the indicated concentrations of dynasore for 15 min and processed for Western blots with MAVS, IκBα and GAPDH antibodies. (D) Bands were subjected to densitometry and expressed as ratio of MAVS or IκBα/GAPDH. (E) Cells were pre-incubated with the proteasome inhibitor MG-132 (10 μM) or DMSO for 30 min in HBSS. Cells were then treated with or without the inhibitor plus or minus dynasore (80 μM) or DMSO for 15 min. Cells were lysed and subjected to Western blotting for MAVS, IκBα and reprobed for GAPDH for loading correction. Note that dynasore-induced reduction in MAVS monomer is not inhibited by MG-132, while dynasore-induced degradation of IκBα is inhibited by MG-132.

activation is likely downstream of MAVS activation in response to dynasore treatment.

Dynasore effect on MAVS is not through RIG-I

RIG-I is a cytoplasmic helicase that binds viral double-stranded RNA and activates mitochondrial MAVS (West *et al.*, 2011). We, therefore, studied whether it is involved in dynasore activation of MAVS. As can be noted in Figure 10, knocking down RIG-I protein with specific siRNAs did not affect dynasore-induced reduction of MAVS and IκBα levels, suggesting that dynasore activates MAVS pathway independent of RIG-I.

Discussion and conclusions

The present studies report the novel observation that dynasore, an agent frequently used to inhibit CME, is able to activate NF-κB and IFN-dependent processes, independent of its effects on endocytosis. Dynasore appears to exert these effects through the mitochondrial adaptor protein MAVS via a mechanism involving activation of the Rho family small GTPase Rac1. The observation that Rac1 is an upstream regulator of MAVS aggregation builds a novel relationship between small GTPase-mediated stress signalling and structural elements of the antiviral machinery. The data also suggest that generation of ROS via NADPH oxidase and mitochondrial oxidases in response to dynasore treatment is responsible for initiating the downstream events. Finally, activation of JNK/SAPK kinase appears to be downstream of MAVS activation and JNK/SAPK leads to activation of NF-κB. This finding sheds some mechanistic insight into the observations reported by Chung *et al.* (2009), which first demonstrated that dynasore was able to induce TGF-β signalling via JNK/SAPK kinase activation.

During viral infection, the MAVS adaptor protein serves a pivotal role in translating upstream sensing of viral infection into a downstream antiviral response. The present studies show that the downstream effects of dynasore treatment

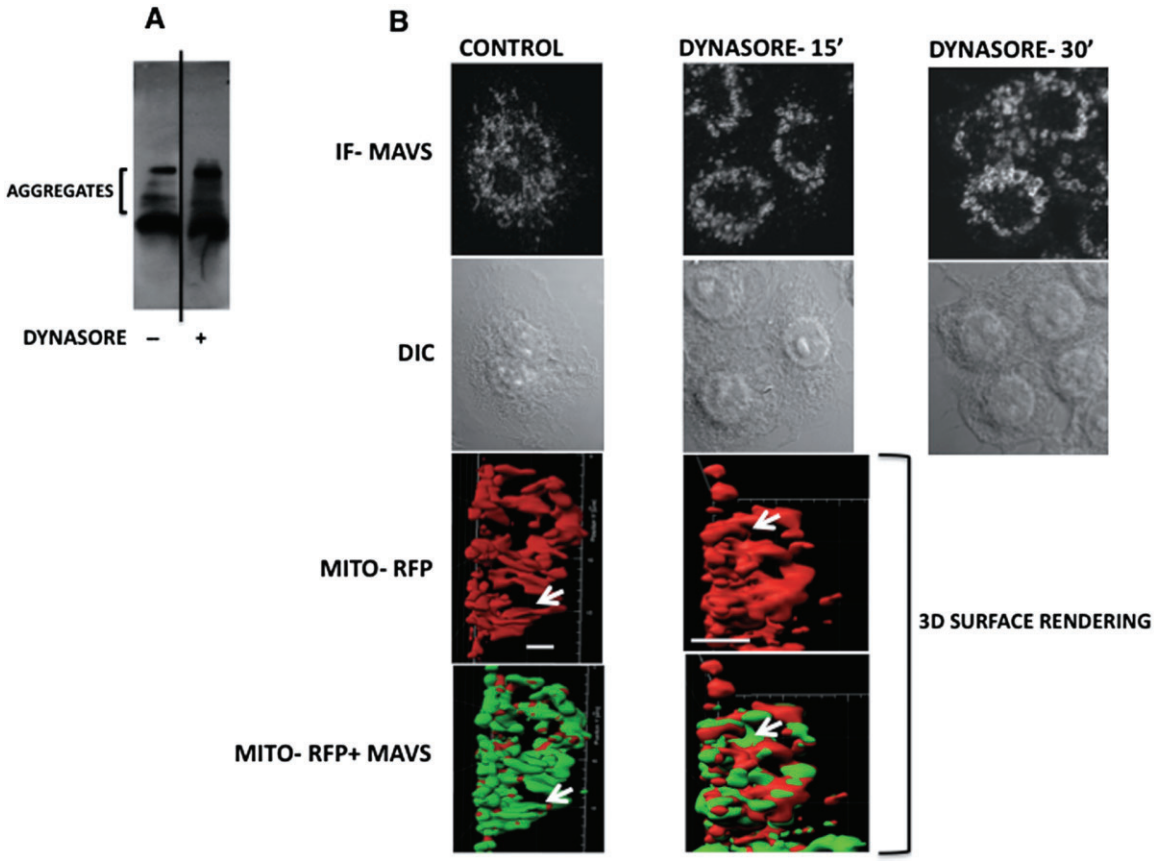

Figure 5

Dynasore treatment causes formation of high molecular weight aggregates of MAVS. (A) SDD-AGE: RAW cells were treated with dynasore (80 μM) or DMSO for 15 min in HBSS. Cell lysates were run on SDD-AGE and immunoblotted with MAVS antibody. (B) Immunofluorescence: cells were treated with dynasore (80 μM) or DMSO for 15 and 30 min in HBSS. Cells were then fixed and subjected to fluorescent confocal microscopy (IF-MAVS) or differential interference contrast microscopy (DIC). Note the disruption of elongated MAVS thread-like structure following treatment with dynasore. Lower two panels: three-dimensional surface rendering colocalization of MAVS (immunofluorescent, green) and mitochondria (Mito-RFP, red) and changes in their structures following treatment with dynasore. Cells were transfected with Mito-RFP plasmid and treated with DMSO or dynasore (80 μM) for 15 min. Images depict side view of micrographs shown in Supporting Information Fig. S4 from Videos S1 and S2 3D surface rendering representing one frame each from control and dynasore-treated cells. Note that in control cells, MAVS covers the majority of the mitochondrial surface area indicating its even distribution on the mitochondrial surface. In dynasore-treated cells, MAVS is redistributed in a polar fashion between the mitochondria and facilitate attachment of individual threads to form multi-organelle structure of mitochondria. Bars represent 5 μm.

involve MAVS. As MAVS is an adaptor protein, which serves as a signalosome for downstream events, its activation is evidenced by virtue of its change in configuration to one which is known to provide a platform for its known antiviral function. Specifically, our data show that dynasore induces the formation of high molecular weight MAVS aggregates and stimulates the formation of MAVS clusters, which appear to bridge the mitochondria. The ability of dynasore to induce MAVS aggregates that are resistant to SDS disaggregation is similar to such property of prions (Hou *et al*., 2011). Hou *et al*. suggest that this 'prion-like' conformational switch is dependent on the caspase recruitment domain (CARD) of MAVS and is essential for downstream antiviral signalling in Sendai virus-treated cells. It is interesting to note that MAVS form prion-like complexes hours after viral infection, while the dynasore effect is much faster as it occurs within minutes after its addition to the cells. The critical role of MAVS in the dynasore-induced activation of NF-κB is supported by the inhibition of NF-κB-luciferase activation following treatment with MAVS siRNA. This treatment was shown to inhibit formation of aggregates in Sendai virus-treated cells.

Dynasore-induced activation of downstream signalling appears to involve the generation of oxidative stress as the antioxidant NAC inhibited NF-κB activation as measured by p65 phosphorylation and NF-κB-luciferase activation. In addition, dynasore itself stimulated release of H_2O_2 from RAW cells into the medium. Using specific inhibitors of cytoplasmic and mitochondrial ROS, oxidants from both NADPH oxidase and mitochondrial oxidases were implicated in the effect. We also investigated a potential upstream target for dynasore's action. The Rho family small GTPase Rac induces activation of NADPH oxidase to generate cytoplasmic ROS

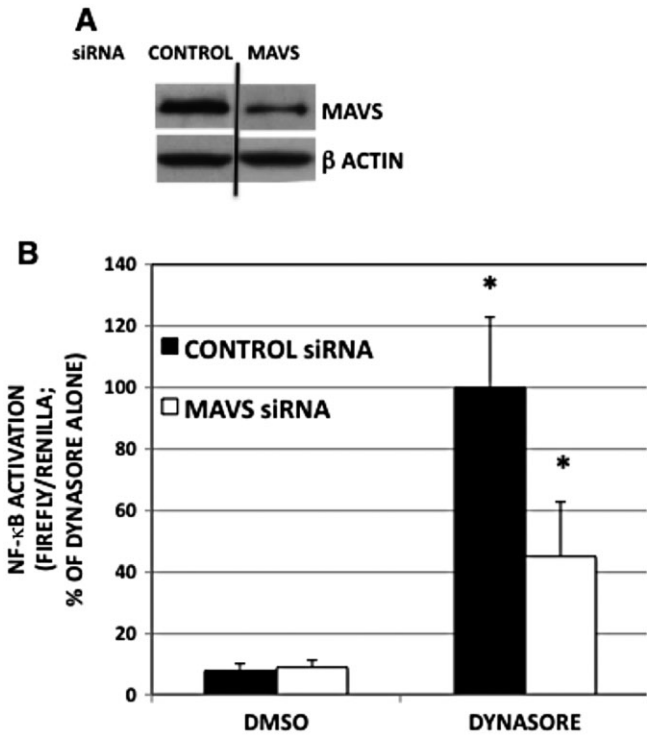

Figure 6

Knock-down of MAVS with specific siRNA reduces dynasore-induced activation of NF-κB-luciferase. (A) To demonstrate the utility of MAVS siRNA, cells were transfected with 10 nM of control or MAVS siRNA overnight. Cells were subjected to Western blotting analysis using MAVS antibody or β-actin antibody for loading control. (B) Cells were transfected with 10 nM of control or MAVS siRNA overnight. Next day, cells were double- transfected with NF-κB-luciferase and renilla-luciferase for 6 h. Cells were treated with dynasore (80 μM) or DMSO for 15 min in HBSS and then kept in 2% FBS-containing medium overnight. ANOVA: $P < 0.002$; d.f. within groups = 12.

(Pick, 2014) and a recent report shows that activated Rac1 translocates to the mitochondria where it accepts electrons from cytochrome c and modulates mitochondrial H_2O_2 production (Osborn-Heaford *et al*., 2012). In the present communication, dynasore was shown to activate Rac; Rac1, but not Rac2, appeared to be involved in the activation of MAVS. The specificity of Rac1 in this effect is consistent with the fact that this isoform is the predominant form found in monocytic cells (Pick, 2014). The mechanism whereby oxidative stress leads to activation of MAVS was not specifically investigated in the present studies. Tal *et al*. (2009) demonstrated that mitochondrial ROS were able to stimulate RIG-I receptors, proteins that are known to promote the activation of MAVS and downstream antiviral cytokines. This does not appear to account for dynasore's mechanism, as knocking down RIG-I did not alter dynasore's effect on MAVS.

Like Chung *et al*. (2009), we show that dynasore is able to induce phosphorylation of JNK. JNK is a well-described downstream target of active Rac and given the activation of Rac1 by dynasore, JNK activation was anticipated. However, the finding that JNK inhibition with SP600125 did not alter MAVS suggests that JNK is positioned downstream of MAVS following dynasore treatment. In support of this interpretation, Seth *et al*. showed that overexpression of HA-MAVS in HEK 293 cells lead to the phosphorylation of JNK and further suggested that this might contribute to the antiviral response through activation of ATF-2 (Seth *et al*., 2005). However, JNK interacts directly with ATF-2 to activate E-selectin (Kaszubska *et al*., 1993). Similarly, JNK was found to be downstream of MAVS via involvement of TRAF6 (Hou *et al*., 2011). An alternative explanation might be that JNK is activated by active Rac and that this represents a separate pathway independent of MAVS, but is one that contributes to the antiviral signalling. Interestingly, dynasore activated both the JNK and the NF-κB pathways and JNK inhibition reduced dynasore-induced NF-κB activation. Generally, these two pathways are seen as functionally antagonistic, with JNK promoting apoptosis, while NF-κB enhancing survival (Nakano, 2004). It has also been recognized that extensive cross-talk occurs between these signalling molecules. To a significant extent, the literature supports the general notion that NF-κB acts as an inhibitor of JNK and precludes the proapoptotic effects of JNK by this mechanism (Nakano, 2004). However, the converse relationship, namely the impact of JNK on the NF-κB pathway has also been shown, although this relationship is less well appreciated. Kim *et al*. demonstrated that Wnt5a activates NF-κB in THP-1 monocytic cells in a JNK-dependent manner (Kim *et al*., 2012). Our work provides further evidence for the positive effects of JNK on NF-κB activation. Together, these studies suggest that the relative relationship of these two signalling molecules in JNK/NF-κB cross-talk is context-dependent (Nakano, 2004). Specifically, our studies suggest the possibility that the NF-κB signalling turned on in a MAVS-dependent manner involves JNK activation. This is consistent with the activation of both pathways during viral infection (Mosallanejad *et al*., 2014). It is noteworthy that SP600125 has been shown to inhibit kinases other than JNK (Bain *et al*., 2003). Further work is required to establish the hierarchy of JNK in the MAVS pathway and to elucidate whether MAVS might bind JNK and could represent a platform channelling the response towards NF-κB activation.

Our studies show that dynasore alters mitochondrial morphology inducing a shift from a thread-like structure to a multi-organelle organization along with a dramatic change in the spatial relationship between MAVS and mitochondria. Regarding the latter, MAVS appears to move from the surface of mitochondria to the intermitochondrial space linking mitochondrial stacks together. The change in mitochondrial morphology, in principle, might be related to a change in mitochondrial dynamics due to alterations in fission and/or fusion (West *et al*., 2011). Indeed, both of these processes may be affected as DRP1 phosphorylation, a reaction provoked by dynasore, has been shown to reduce the mitochondria-fragmenting activity of this GTPase (Knott *et al*., 2008), while JNK phosphorylation has been shown to promote mitofusin (MFN) degradation and thereby interferes with fusion (Guillaume *et al*., 2012). However, it should be emphasized that morphological changes may arise, at least partly, independently of fusion and fission, as aggregated MAVS themselves have the capacity to link mitochondrial threads side by side, as observed in virus-infected cells (Xu *et al*., 2014) and in dynasore-treated cells in the present study. Moreover, the

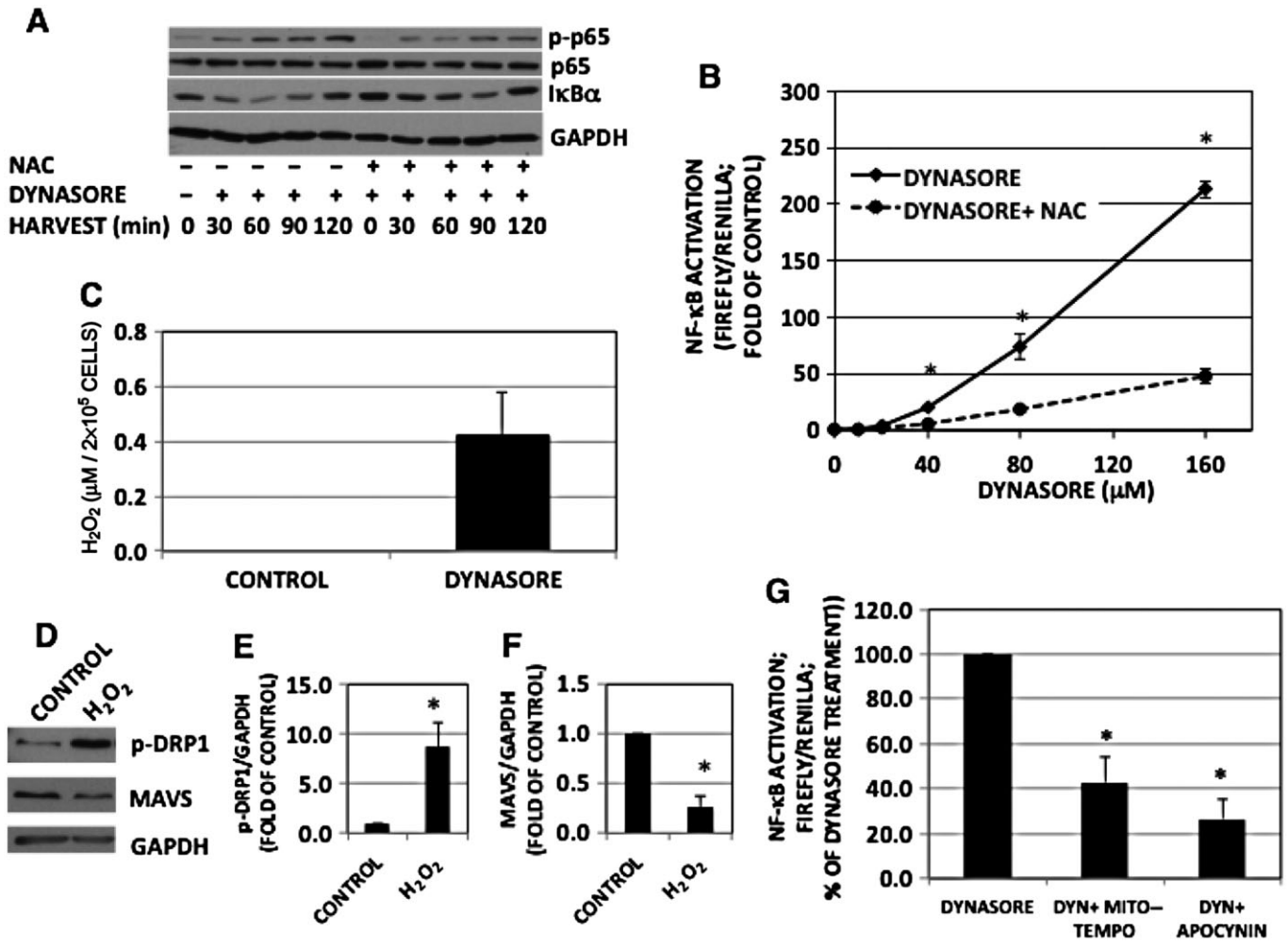

Figure 7

The effect of dynasore is mediated by ROS. (A) Western immunoblot of NF-κB-p-p65 and IκBα: cells were pre-incubated with NAC (100 mM) or vehicle for 30 min in HBSS, followed by dynasore (80 μM) or DMSO for additional 15 min. Cells were then treated in 2% FBS with the inhibitors for the times indicated. NF-κB-p-p65 and IκBα representative blots were from two independent separate experiments. Therefore, loading was ascertained by reprobing with p65 or GAPDH respectively. Note the inhibition of dynasore induction of NF-κB-p-p65 and IκBα degradation with NAC, suggesting that dynasore induction is mediated by ROS. (B) NF-κB-luciferase: cells were transfected and maintained as described in the Methods section ($n = 3$). (C) H_2O_2 assay: cells were plated and treated as described earlier. Aliquots of conditioned media were assayed for H_2O_2 using Amplex red kit. Note the enhanced levels of H_2O_2 in dynasore-treated cells ($n = 3$). (D) Western immunoblot showing that H_2O_2 increase p-DRP1 and reduces MAVS monomer levels. Cells were treated with 300 μM H_2O_2 for 15 min and processed for Western blotting for p-DRP1, MAVS and GAPDH. (E, F) Densitometry of blots shown in panel D: bands were scanned, corrected for GAPDH levels and normalized to the corresponding controls. Increase in p-DRP1 (E) and decrease in MAVS (F) are statistically different ($P < 0.03$; $n = 3$) from DMSO-treated control. (G) NF-κB-luciferase: cells were pretreated for 20 min with Mito-Tempo (25 μM; inhibitor of mitochondrial ROS), apocynin (600 μM; inhibitor of NADPH oxidase) or DMSO in HBSS, followed by treatment with dynasore (80 μM) for another 15 min. Cells were then treated with the inhibitors in 2% FBS overnight and processed for luciferase measurement. Both ROS inhibitors reduced dynasore-induced activation of NF-κB-luciferase (ANOVA: $P < 3 \times 10^{-6}$; d.f. within groups = 12).

functional consequences of MAVS-induced direct and indirect (fusion- or fission-modifying) changes are complex and are not well understood. For example, on one hand, MFN2 was found to bind to and form aggregates with MAVS to inhibit antiviral signalling (Yasukawa *et al.*, 2009), while on the other, MFN2-mediated mitochondrial fusion was claimed to be crucial for MAVS-mediated induction of interferons and pro-inflammatory cytokines (Koshiba *et al.*, 2011). Our data show that dynasore mimics many of the morphological and functional effects of viral induction including MAVS aggregation, a characteristic reorganization of the MAVS–mitochondrion relationship and the induction of key cytokines.

Dynasore enhanced the NF-κB pathway as measured by a luciferase reporter assay. Combined treatment of dynasore and LPS elicited a synergistic effect on NF-κB. We surmise that

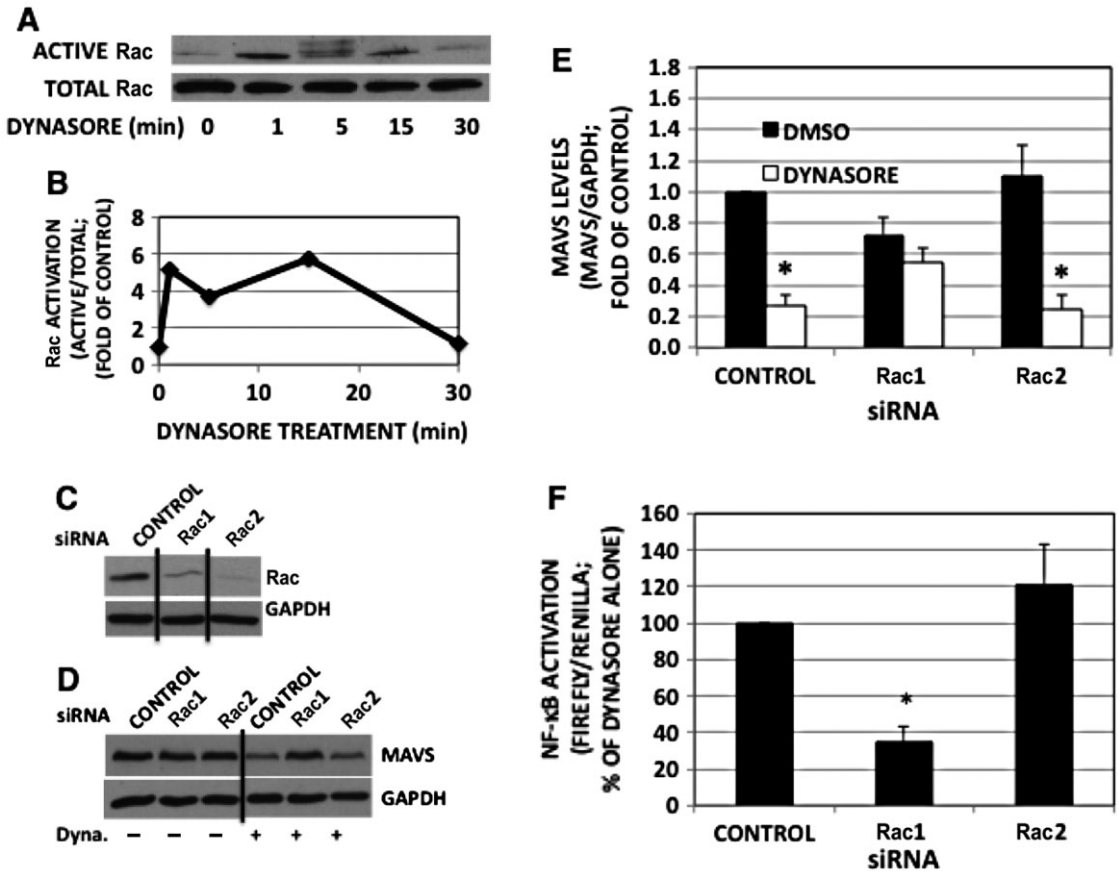

Figure 8

Dynasore induces Rac activation and Rac1 down-regulation mitigates dynasore-induced MAVS reduction and NF-κB activation. (A) RAW cells were maintained as described in the Methods section and treated with dynasore for the times indicated. Cell extracts were subjected to Rac activation assay. The top blot shows Rac precipitated (active Rac), while the bottom blot shows Rac in the corresponding total cell lysates. (B) Densitometry of active Rac normalized with total Rac depicted in panel A. (C) Western blot demonstrating the utility of Rac siRNAs used. Cells were transfected with the siRNAs for 24 h and subjected to Western blot with Rac antibody. Note the knockdown of both Rac1 and Rac2 with the specific siRNA used. (D) Western blot: RAW cells were transfected with siRNA for 24 h. Cells were treated with dynasore (80 μM) or DMSO for 15 min in HBSS, extracted and subjected to Western immunoblot with anti-MAVS antibody. Blots were reprobed for GAPDH for normalization. (E) Densitometric analysis of experiments depicted in panel B of MAVS/GAPDH ratios. (ANOVA: $P < 6 \times 10^{-4}$; d.f. within groups = 18). (F) NF-κB-luciferase assay: cells were transfected with siRNA and luciferase plasmids and treated with dynasore as indicated earlier. Data are expressed as percentage of dynasore alone-treated cells marked as CONTROL. (ANOVA: $P < 2 \times 10^{-3}$; d.f. within groups = 7).

the reason for the synergism of the combined treatment in the NF-κB pathway is due to the activation of two pathways, namely LPS induces the TLR4/MyD88-MAL pathway (the TLR4/TRAM-TRIF pathway being blocked by dynasore) and dynasore activates the MAVS mitochondrial pathway. Consistent with this conclusion is the fact that polymyxin B treatment of the cells exposed to LPS plus dynasore reduced activation of NF-κB-luciferase to the level of that seen with dynasore alone. Therefore, further studies are warranted to determine whether the two stimuli might exhibit positive cross-talk between the bacterially and virally induced signalling pathways.

In summary, dynasore appears to induce a signalling cascade that is independent of its effects on CME. These include activation of MAVS and its downstream antiviral pathways. Efficient activation of the innate immune response through MAVS is essential for successful elimination of viral propagation. This suggests the possibility that activation of immune response pathways by dynasore is similar to that of viral infection and could be considered a potential antiviral therapeutic strategy. Dynasore is currently a commonly used pharmacological agent for studies of CME. The data presented in this communication underscore the care that should be taken in interpretation of experiments that use dynasore as the sole inhibitor of CME. Finally, the present work also suggests that dynasore may be used as an efficient and fast MAVS pathway activator in future studies.

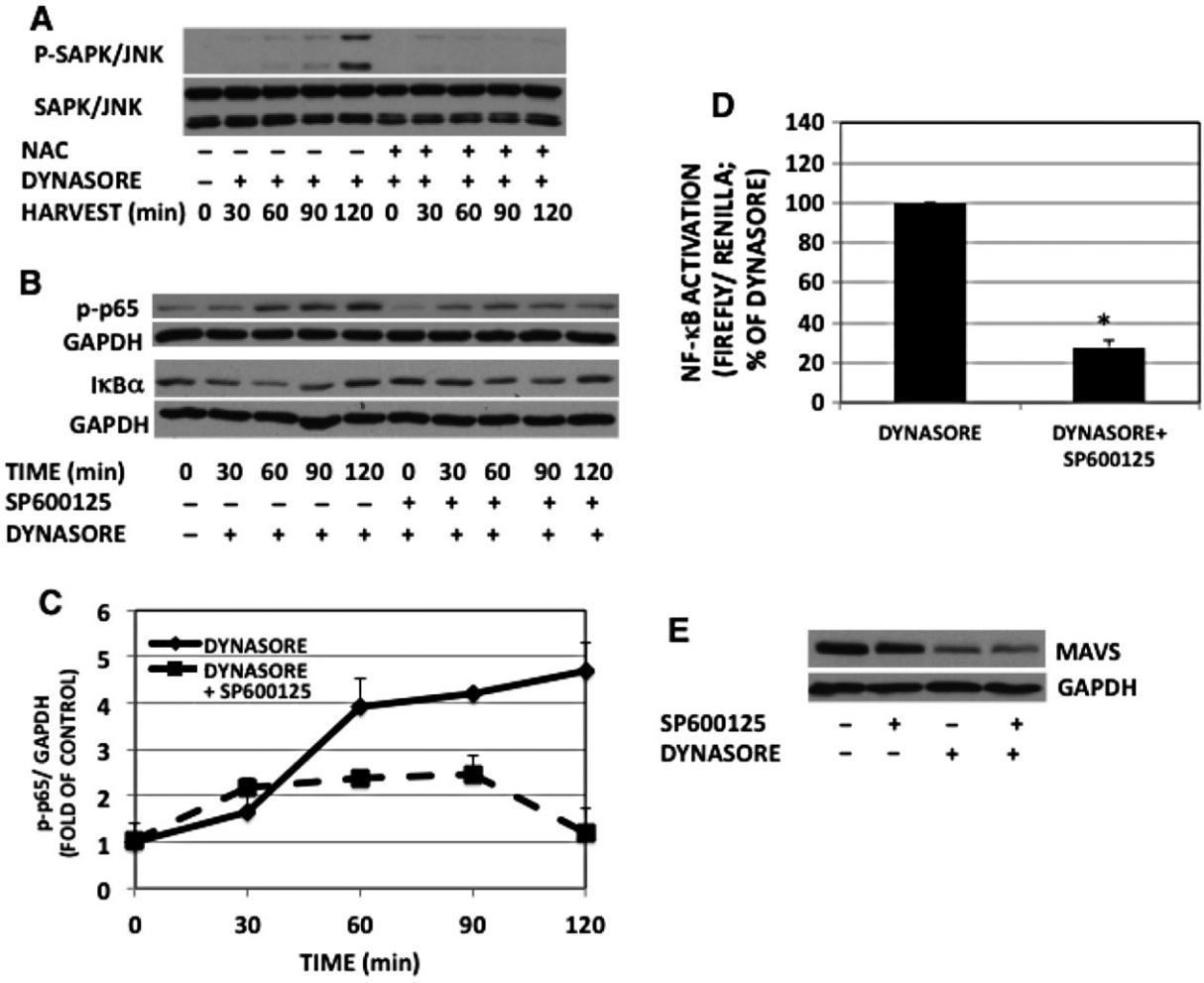

Figure 9

Dynasore effect on NF-κB- p65 activation is mediated by SAPK/JNK. (A) Western immunoblot of phospho-SAPK/JNK: RAW cells were pretreated with or without NAC for 30 min, followed by incubation with dynasore (80 μM) for the times indicated in 2% FBS. Note the inhibition of dynasore-induced SAPK/JNK phosphorylation by NAC. (B) Western immunoblot of NF-κB-p-p65 and IκBα: cells were pre-incubated for 30 min with the SAPK/JNK inhibitor SP600125 (10 μM) or DMSO in HBSS, then dynasore (80 μM) was added to the cells for the times indicated. NF-κB-p-p65 and IκBα representative blots were from two independent separate experiments. Therefore, loading was ascertained by reprobing each corresponding blot with GAPDH. (C) Densitometry of blots of NF-κB-p-p65 and GAPDH depicted in panel B: NF-κB-p-p65 levels were normalized with GAPDH corresponding bands. (ANOVA: $P < 2 \times 10^{-5}$; d.f. within groups = 20). (D) NF-κB-luciferase: SP600125 pretreatment of cells inhibited dynasore-induced enhancement of NF-κB-luciferase ($P < 3 \times 10^{-5}$; $n = 3$; Student's t-test). (E) Western immunoblot of MAVS: cells were pre-incubated for 30 min with SP600125 (10 μM) or DMSO in HBSS, then dynasore (80 μM) or DMSO was added to the cells for an additional 15 min. Cell extracts were subjected to Western blot with anti-MAVS and GAPDH antibodies.

Acknowledgements

This work was supported by Canadian Institutes of Health Research (CIHR) grant MOP 37779 to O. D. R. and Natural Sciences and Engineering Research Council of Canada (NSERC) grants RGPIN 327407-12 and RGPIN 227908-13 to K. S. and A. K. respectively.

Author contributions

M. A., O. D. R. and A. K. conceptualized and designed the research study. O. D. R., A. K. and K. S. contributed essential reagents, tools and funding. M. A., C. D. C.-O., Q. D. and M. R. performed the technical aspects of the studies. M. A., O. D. R., A. K., C. D. C.-O. and K. S. analysed and collated the data and wrote the manuscript.

Conflict of interest

None.

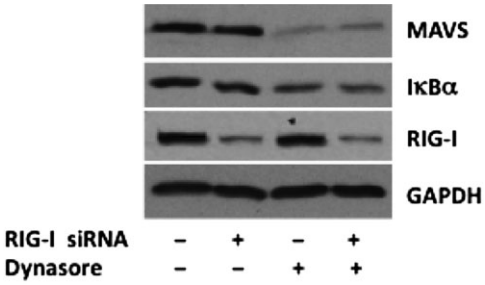

Figure 10

Western blot analysis suggesting that dynasore's effect on MAVS and IκBα is not mediated by RIG-I; cells were transfected with negative control siRNA or with a mixture of specific RIG-I siRNAs. Next day, cells were starved for 15 min in HBSS followed by 15 min treatment with vehicle DMSO or dynasore (80 μM). Note that dynasore's effect on MAVS and IκBα is not affected by knockdown of RIG-I.

References

Ailenberg M, Rotstein OD (2011). Oxidative stress enhances pro-inflammatory signal cascade by increasing association of TLR4 with TIRAP (MAL), enhancing of TIRAP-MyD88 signaling pathway, and inhibiting of the TRAM-TRIF signaling pathway. Mol Biol Cell 22 (Suppl.): Abstract number 606.

Ailenberg M, Di Ciano-Oliveira C, Rotstein OD (2011). Dynasore – an inhibitor of clathrin-mediated endocytosis (CME) is a potent activator of NFκB independent of CME. Mol Biol Cell 22 (Suppl.): Abstract number 614.

Alexander SPH, Benson HE, Faccenda E, Pawson AJ, Sharman JL, Spedding M *et al.* (2013a). The Concise Guide to PHARMACOLOGY 2013/14: catalytic receptors. Br J Pharmacol. 170: 1676–1705.

Alexander SPH, Benson HE, Faccenda E, Pawson AJ, Sharman JL, Spedding M *et al.* (2013b). The Concise Guide to PHARMACOLOGY 2013/14: enzymes. Br J Pharmacol. 170: 1797–1867.

Bagriantsev SN, Kushnirov VV, Liebman SW (2006). Analysis of amyloid aggregates using agarose gel electrophoresis. Methods Enzymol 412: 33–48.

Bain J, McLauchlan H, Elliott M, Cohen P (2003). The specificities of protein kinase inhibitors: an update. Biochem J 371: 199–204.

Bonham KS, Orzalli MH, Hayashi K, Wolf AI, Glanemann C, Weninger W *et al.* (2014). A promiscuous lipid-binding protein diversifies the subcellular sites of toll-like receptor signal transduction. Cell 156: 705–716.

Castanier C, Zemirli N, Portier A, Garcin D, Bidère N, Vazquez A *et al.* (2012). MAVS ubiquitination by the E3 ligase TRIM25 and degradation by the proteasome is involved in type I interferon production after activation of the antiviral RIG-I-like receptors. BMC Biol 10: 44–56.

Chung C-L, Sheu J-R, Liu H-E, Chang S-C, Chou Y-C, Chen W-L *et al.* (2009). Dynasore, a dynamin inhibitor, induces PAI-1 expression in MeT-5A human pleural mesothelial cells. Am J Respir Cell Mol Biol 40: 692–700.

Finkel T (2012). Signal transduction by mitochondrial oxidants. J Biol Chem 287: 4434–4440.

Guillaume P, Leboucher GP, Tsai YC, Yang M, Shaw KC, Zhou M *et al.* (2012). Stress-induced phosphorylation and proteasomal degradation of mitofusin 2 facilitates mitochondrial fragmentation and apoptosis. Mol Cell 47: 547–557.

Hordijk PL (2006). Regulation of NADPH oxidases: the role of Rac proteins. Circ Res 98: 453–462.

Hou F, Sun L, Zheng H, Skaug B, Jiang Q-X, Chen ZJ (2011). MAVS forms functional prion-like aggregates to activate and propagate antiviral innate immune response. Cell 146: 448–461.

Howes MT, Kirkham M, Riches J, Cortese K, Walser J, Simpson F *et al.* (2012). Clathrin-independent carriers form a high capacity endocytic sorting system at the leading edge of migrating cells. J Cell Biol 190: 675–691.

Husebye H, Halaas O, Stenmark H, Tunheim G, Sandanger O, Bogen B *et al.* (2006). Endocytic pathways regulate Toll-like receptor 4 signaling and link innate and adaptive immunity. EMBO J 25: 683–692.

Kaszubska W, van Huijsduijnen RH, Ghersa P, Deraemy-Schenk A-M, Chen BPC, Hai T *et al.* (1993). Cyclic AMP-independent ATF family members interact with NF-κB and function in the activation of the E-selectin promoter in response to cytokines. Mol Cell Biol 13: 7180–7190.

Kim J, Chang W, Jung Y, Song K, Lee I (2012). Wnt5a activates THP-1 monocytic cells via a β-catenin-independent pathway involving JNK and NF-κB activation. Cytokine 60: 242–248.

Kirchhausen T, Macia E, Pelish HE (2008). Use of dynasore, the small molecule inhibitor of dynamin, in the regulation of endocytosis. Methods Enzymol 438: 77–93.

Knott AB, Perkins G, Schwarzenbacher R, Bossy-Wetzel E (2008). Mitochondrial fragmentation in neurodegeneration. Nat Rev Neurosci 9: 505–518.

Koshiba T, Yasukawa K, Yanagi Y, Kawabata S-I (2011). Mitochondrial membrane potential is required for MAVS-mediated antiviral signaling. Sci Signal 4: ra7.

Macia E, Ehrlich M, Massol R, Boucrot E, Brunner C, Kirchhausen T (2006). Dynasore, a cell- permeable inhibitor of dynamin. Dev Cell 10: 839–850.

Masszi A, Speight P, Charbonney E, Lodyga M, Nakano H, Szászi K *et al.* (2010). Fate-determining mechanisms in epithelial-myofibroblast transition: major inhibitory role for Smad3. J Cell Biol 188: 383–399.

Mosallanejad K, Sekine Y, Ishikura-Kinoshita S, Kumagai K, Nagano T, Matsuzawa A *et al.* (2014). The DEAH-box RNA helicase DHX15 activates NF-{kappa}B and MAPK signaling downstream of MAVS during antiviral responses. Sci Signal 7: ra40.

Nakano H (2004). Signaling crosstalk between NF-κB and JNK. Trends Immunol 25: 402–405.

Osborn-Heaford HL, Ryan AJ, Shubha Murthy S, Racila A-M, Chao He C, Jessica C *et al.* (2012). Mitochondrial rac1 GTPase import and electron transfer from cytochrome c are required for pulmonary fibrosis. J Biol Chem 287: 3301–3312.

Papia G, Fan J, Kapus A, Szaszi K, Marshall JC, Tawadros P *et al.* (2011). Altered inhibitory κBα expression in LPS-stimulated alveolar macrophages following resuscitated hemorrhagic shock. Shock 35: 171–177.

Pawson AJ, Sharman JL, Benson HE, Faccenda E, Alexander SP, Buneman OP *et al.*; NC-IUPHAR (2014). The IUPHAR/BPS Guide to PHARMACOLOGY: an expert-driven knowledgebase of drug targets and their ligands. Nucleic Acids Res 42 (Database Issue): D1098–D1106.

Pick E (2014). Role of the Rho GTPase Rac in the activation of the phagocyte NADPH oxidase: outsourcing a key task. Small GTPases 5: 1, e27952, DOI: 10.4161/sgtp.27952.

Powers KA, Szászi K, Khadaroo RG, Tawadros PS, Marshall JC, Kapus A *et al*. (2006). Oxidative stress generated by hemorrhagic shock recruits Toll-like receptor 4 to the plasma membrane in macrophages. J Exp Med 203: 1951–1961.

Sanada T, Takaesu G, Mashima R, Yoshida R, Kobayashi T, Yoshimura A (2008). FLN29 deficiency reveals its negative regulatory role in the toll-like receptor (TLR) and retinoic acid-inducible gene I (RIG-I)-like helicase signaling pathway. J Biol Chem 283: 33858–33864.

Seth RB, Sun L, Ea C-K, Chen ZJ (2005). Identification and characterization of MAVS, a mitochondrial antiviral signaling protein that activates NF-κB and IRF3. Cell 122: 669–682.

Szászi K, Jones JJ, Nathens AB, Lo A-Y, Marsden PA, Kapus A *et al*. (2005). Glutathione depletion inhibits lipopolysaccharide- induced intercellular adhesion molecule 1 synthesis. Free Radic Biol Med 38: 1333–1343.

Tal MC, Sasai M, Lee HK, Yordy B, Shadel GS, Iwasaki A (2009). Absence of autophagy results in reactive oxygen species-dependent amplification of RLR signaling. Proc Natl Acad Sci U S A 106: 2770–2775.

Waheed F, Dan Q, Amoozadeh Y, Zhang Y, Tanimura S, Speight P *et al*. (2013). Central role of the exchange factor GEF-H1 in TNF-α–induced sequential activation of Rac, ADAM17/TACE, and RhoA in tubular epithelial cells. Mol Biol Cell 24: 1068–1082.

West AP, Shadel GS, Ghosh S (2011). Mitochondria in innate immune responses. Nat Rev Immunol 11: 389–402.

Xu H, He X, Zheng H, Huang LJ, Hou F, Yu Z *et al*. (2014). Structural basis for the prion-like MAVS filaments in antiviral innate immunity. eLife 3: e01489.

Yasukawa K, Oshiumi H, Takeda M, Ishihara N, Yanagi Y, Seya T *et al*. (2009). Mitofusin 2 inhibits mitochondrial antiviral signaling. Sci Signal 2: ra47.

Supporting information

Additional Supporting Information may be found in the online version of this article at the publisher's web-site:

http://dx.doi.org/10.1111/bph.13162

Figure S1 CME inhibitors prevent rhodamine-transferrin endocytosis but do not activate NF-κB, p65 or IκBα. Effect of inhibitors used in this study on cell viability. (A) Fluorescent microscopy: cells were treated for 15 min in HBSS with DMSO (Control), dynasore (80 μM), MiTMAB (10 μM) or Pitstop-2 (25 μM). Cells were then allowed to bind rhodamine-transferrin on ice and transferred to 370°C for 5 min. (B) NF-κB-luciferase: cells were treated with Pitstop-2 at the concentration indicated. (C) Western immunoblot: RAW cell were treated with DMSO (Control), dynasore (80 μM), MiTMAB (10 μM) or Pitstop-2 (25 μM) for 2 h. Membranes were probed with p-p65, IκBα and GAPDH antibodies. Note that only dynasore enhances p-p65 and induces degradation of IκBα. (D, E) Cell viability: cells were treated with the inhibitors for 2 h (D) or 24 h (E) and subjected to trypan blue dye exclusion assay. Note that after 2 h exposure of all treatments, more than 99% of cells were viable. After 24 h exposure, dynasore and NAC treatment yielded more than 98% viable cells, Pitstop-2 yielded 62% viable cells and after MiTMAB treatment, no viable cells were present.

Figure S2 Dynasore effect is not through TLR4 pathway. (A) RAW cells co-transfected with NF-κB and renilla luciferase plasmids were pre-incubated with IRAK 1/4 inhibitor (10 μM) and dynasore (80 μM) and incubated with or without the inhibitors and LPS (15ng·mL^{-1}) overnight. Note that while IRAK 1/4 inhibitor inhibits LPS-induced NF-κB-luciferase activation, it does not affect dynansore-induced NF-κB-luciferase activation. ANOVA: $P < 0.002$; d.f. within group = 12, $n = 3$. Asterisk denotes difference ($P < 0.05$) between LPS and LPS + IRAK 1/4 inhibitor. (B) HEK cells that do not express TLR4, respond to dynasore by activation of NF-κB similar to RAW cells. Bars represent the mean plus SEM. Dynasore treatment is statistically different from DMSO-treated control ($P < 0.009$; $n = 3$).

Figure S3 Colocalization of MAVS (immunofluorescent, green) and mitochondria (Mito-RFP, red) and changes in their structures following treatment with dynasore. Cells were transfected with Mito-RFP plasmid, maintained and treated as described in the Methods section. Differential interference contrast (DIC) microscopy is depicted on the right. Note the disruption of thread-like structure evident both in mitochondria and MAVS staining. Arrows in dynasore-treated cells depict MAVS puncta similar to that observed in virus-infected cells (Xu *et al*., 2014). Lower panel in the figure depicts enlarged aggregate marked in arrows in the middle panel of dynasore-treated cells. Note also that MAVS and mitochondria are not completely colocalized. Bars at the upper two panels represent 5 μM and at the lower panel 1 μM.

Figure S4 Colocalization of MAVS (immunofluorescent, green) and mitochondria (Mito-RFP, red) and changes in their structures following treatment with dynasore. (A) Cells were transfected with Mito-RFP plasmid, maintained and treated as described in the Methods section. Images from Videos S1 and S2 3D surface rendering represent one frame each from control (upper panel) and dynasore-treated cells (lower panel). Note that in control cells, MAVS covers the majority of the mitochondrial surface area indicating even distribution on the mitochondrial surface (upper panel, arrow). In dynasore-treated cells, MAVS undergoes redistribution to the area between the mitochondria (lower panel, arrow). Note in upper panel the two non-transfected cells (asterisks), which stain for MAVS but not mitochondria. Bars represent 5 μM.

Figure S5 Dynasore causes phosphorylation of mitochondrial DRP1 on Ser 637, but dynasore's effect is not due to the inhibition of DRP1 GTPase activity. (A) Western blot: cells were treated with 80 μM dynasore in HBSS for the times indicated. For loading correction, nitrocellulose membranes were reprobed with GAPDH or DRP1. (B) Bands in panel A were subjected to densitometry and expressed as ratio of p-DRP1/GAPDH. (C) Western blot showing that MIDVI-1 (10 μM; specific inhibitor of DRP1 GTPase activity) does not influence MAVS levels and DRP1 phosphorylation. (D, E) Densitometry of blots corrected to GAPDH and normalized to DMSO-treated control. ANOVA: $P < 8 \times 10^{-5}$ for p-DRP1 and $P < 0.04$ for MAVS; d.f. within groups = 9.

Video S1 and S2 Videos of 3D surface rendering of control and dynasore treatment. Slices of confocal images of control

(S1) and dynasore-treated cells (S2) were stacked into 3D images and underwent surface scanning. Images were rotated 360° with red channel alone, representing Mito-RFP (mitochondria-specific staining). Images were rotated again 360° with both red (mitochondria) and green (MAVS) channels on. Note that in control cells, MAVS covers the majority of the mitochondria surface area indicating even distribution on its surface. In dynasore-treated cells, MAVS undergoes polarized redistribution to the area between the mitochondria. Note that some cells in both videos were not transfected with the Mito-RFP plasmid and therefore show staining only for MAVS. The grids in the images represent 5 μm.